Theoretical study on dispersion compensation in air-core Bragg fibers

George Ouyang, Yong Xu, and Amnon Yariv

G. Ouyang is with Department of Electrical Engineering, California Institute of Technology, MS 136-93, Pasadena, California 91125

ouyang@its.caltech.edu

Abstract: In a previous paper we developed a matrix theory that applies to any cylindrically symmetric fiber surrounded by Bragg cladding. Using this formalism, along with Finite Difference Time Domain (FDTD) simulations, we study the waveguide dispersion for the $m = 1$ mode in an air-core Bragg fiber and showed it is possible to achieve very large negative dispersion values ($\sim$ -20,000 ps/(nm.km)) with significantly reduced absorption loss and non-linear effects.

© 2002 Optical Society of America

OCIS codes: (060.2330) Fibers optics communications; (230.1480) Bragg reflectors

References and links

1. P. Yeh, A. Yariv, and E. Marom, "Theory of Bragg fiber," J. Opt. Soc. Am. **68**, 1196-1201, (1978).
2. Y. Fink, D. J. Ripin, S. Fan, C. Chen, J. D. Joannopoulos, and E. L. Thomas, "Guiding optical light in air using an all-dielectric structure," J. Lightwave Technol. **17**, 2039-2041, (1999).
3. M. Miyagi, A. Hongo, Y. Aizawa, and S. Kawakami, "Fabrication of germanium-coated nickel hollow waveguides for infrared transmission," Appl. Phys. Lett. **43**, 430-432, (1983).
4. N. Croitoru, J. Dror, and I. Gannot, "Characterization of hollow fibers for the transmission of infrared radiation," Appl. Opt. **29**, 1805-1809, (1990).
5. R. F. Cregan, B. J. Mangan, J. C. Knight, T. A. Birks, P. St. J. Russell, P. J. Roberts, and D. C. Allan, "Single-mode photonic band gap guidance of light in air," Science **285**, 1537-1539, (1999).
6. M. Ibanescu, Y. Fink, S. Fan, E. L. Thomas, and J. D. Joannopoulos, "An all-dielectric coaxial waveguide," Science **289**, 415-419, (2000).
7. Y. Xu, R. K. Lee, and A. Yariv, "Asymptotic analysis of Bragg fibers," Opt. Lett. **25**, 1756-1758, (2000).
8. G. Ouyang, Y. Xu, and A. Yariv, "Comparative study of air-core and coaxial Bragg fibers: single-mode transmission and dispersion characteristics," Opt. Express **9**, 733-747, (2001). http://www.opticsexpress.org/abstract.cfm?URI=OPEX-9-13-733
9. S. G. Johnson et al., "Low-loss asymptotically single-mode propagation in large-core OmniGuide fibers," Opt. Express **9**, 748-779, (2001). http://www.opticsexpress.org/abstract.cfm?URI=OPEX-9-13-748
10. Y. Xu, G. Ouyang, R. Lee, and A. Yariv, "Asymptotic matrix theory of Bragg fibers," J. Lightwave Technol. **20**, 428-440, (2002).
11. A. Vengsarkar and W. A. Reed, "Dispersion-compensating single-mode fibers: efficient designs for first- and second-order compensation," Opt. Lett. **18**, 924-926, (1993).
12. A. Bjarklev, T. Rasmussen, O. Lumholt, K. Rottwitt, and M. Helmer, "Optimal design of single-cladded dispersion-compensating optical fibers," Opt. Lett. **19**, 457-459, (1994).
13. B. Jopson and A. Gnauck, "Dispersion compensation for optical fiber systems," IEEE Comm. Mag. **33**, 96-102, (1995).
14. Onishi M, Kashiwada T, Ishiguro Y, Nishimura M, and Kanamori H, "High-performance dispersion-compensating fibers," Fiber Integ. Opt. **16**, 277-285, (1997).
15. C. Bradford, "Managing chromatic dispersion increases bandwidth," Laser Focus World, February (2001).
16. M.R.C. Caputo and M.E. Gouvea, "Dispersion slope effects of the compensation dispersion fiber for broadband dispersion compensation in the presence of self-phase modulation," Laser Focus World, February (2001).
17. P. Yeh, A. Yariv, and C. Hong, "Electromagnetic propagation in periodic stratified media. I. General theory," J. Opt. Soc. Am. **67**, 423-438, (1977).

18. K. S. Yee, "Numerical solution of initial boundary value problems involving Maxwell's equations in isotropic media," IEEE Trans. Antennas Propag. **AP-14**, 302-307, (1966).
19. J. P. Berenger, "A perfectly matched layer for the absorption of electromagnetic waves," J. Computat. Phys. **114**, 185-200, (1994).
20. S. D. Gedney, "An anisotropic perfectly matched layer-absorbing medium for the truncation of FDTD lattices," IEEE Trans. Antennas Propag. **44**, 1630-1639, (1996).
21. F. Zepparelli, P. Mezzanotte, F. Alimenti, L. Roselli, R. Sorrentino, G. Tartarini, and P. Bassi, "Rigorous analysis of 3D optical and optoelectronic devices by the compact-2D-FDTD method." Opt. and Quantum Electron. **31**, 827-841, (1999)

1   Introduction

The idea of confining light in a Bragg fiber was first proposed by Yeh et. al. in [1]. Unlike conventional fibers, which guide light through total internal reflection, Bragg fibers achieve light confinement through Bragg reflection. Since Bragg fibers and conventional optical fibers utilize different guiding mechanisms, it is not surprising that Bragg fibers offer many interesting features that are difficult to achieve in conventional fibers. One such example is the possibility of guiding light in air, which has attracted much recent interest [2]-[10]. In a Bragg fiber with large cladding index contrast, light can be confined mostly within the center air core, which can lead to lower absorption loss and reduce the threshold for nonlinear effects [5]. Another area of particular interest is the dispersion characteristics of the air-core Bragg fiber. Johnson et al. [9] have shown that by making the air core sufficiently large, arbitrarily small group velocity dispersions can be achieved for the TE_{01} mode (D $\sim$ 12ps/(nm.km) has been demonstrated), as dispersion D in this case scales as $1/r_{core}^2$, where r_{core} is the core radius. In this paper we focus on a different application: dispersion compensation, for which a large, negative dispersion value is desired. Apparently a different approach should be used in our case, since large dispersion values are generally associated with small core radii.

For years researchers have proposed various schemes to compensate chromatic dispersion using DCFs [11]-[15], with dispersion values D typically ranging up to -1,000 ps/(ns.km). Since none of the above-mentioned schemes guide light in air, they inevitably suffer from absorption loss and nonlinearity effects such as self-phase modulation and four-wave mixing [16]. The degree to which these undesirable effects undermine the performance of the DCFs depends on each particular design. In the following sections we will show that it is theoretically possible to design a Bragg fiber that not only guides light in air, but also produces large negative dispersions ($\sim$ -20,000 ps/(nm.km)).

2   Theoretical analysis

In Ref. [10] we developed a general matrix theory for cylindrically symmetric waveguides with Bragg claddings. In this theory, an arbitrary number of inner dielectric layers, called the "inner region" (IR)[1], are treated exactly, whereas the outside cladding layers, called the "outer region" (OR), are approximated in the asymptotic limit. Approximate mode equations were also derived by matching the boundary conditions at the interface between the IR and the OR, whose accuracy can be improved arbitrarily by including more layers in the IR. For the sake of simplicity, we begin our analysis of air-core Bragg fiber by matching boundary conditions at the air core boundary and improve the accuracy of our results later.

Consider the generic air-core Braggg fiber given in Fig. 1, the mode dispersion relations depend on all five parameters: n_1, n_2, r_{core}, r_1 and r_2. In the limit of large radius,

---

[1]In Ref. [10] it is called the "core region", but we decide to change its name to "inner region" so as not to confuse it with the actual fiber core.
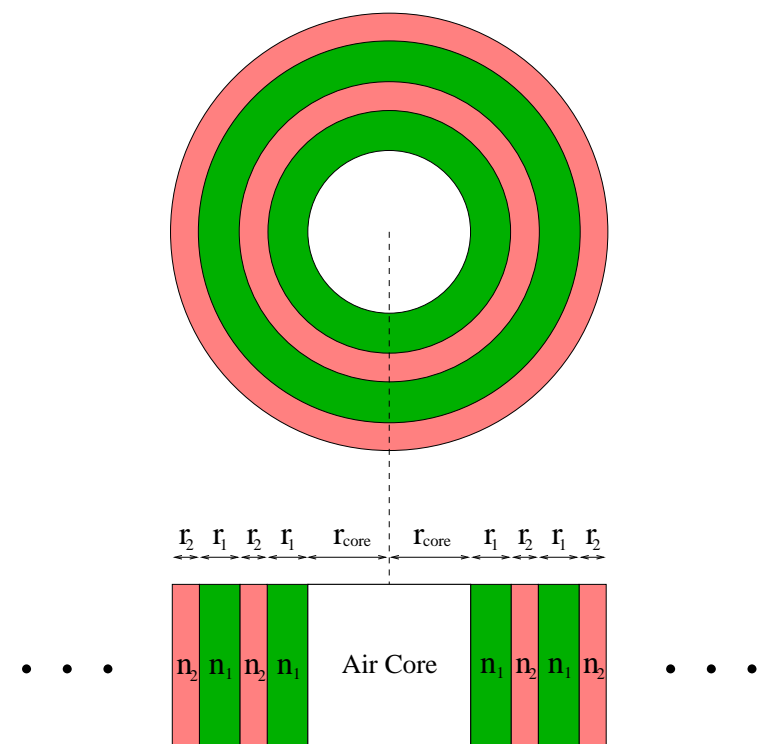
Fig. 1. Schematic of an air-core Bragg fiber. The fiber cladding consists of alternating
layers of dielectric media with high and low refractive indices.

the circular Bragg fiber approaches a planar Bragg stack, whose band diagrams and
mode equations can be found in standard literature [17]. Hence for low-loss transmis-
sion it is necessary to have the Bragg fiber modes to fall inside the TE and/or TM band
gap(s) of the corresponding Bragg stack, whichever is applicable.

   We start with a large index contrast between the cladding layers, so as to result in
a large band gap. We choose $n_1 = 4.6$ and $n_2 = 1.5$, just as in Ref. [10] and we try
different combinations of $\{r_{core}, r_1, r_2\}$ until we find a single-mode frequency window
in which only $m = 1$ modes with negative dispersion exist, where m is the azimuthal
index. Note in general modes in a cylindrically symmetric waveguide are designated by
two mode numbers, one radial and one azimuthal. In this paper we discuss only modes
with the lowest radial mode number – all higher-order modes have been "pushed" out
of the band gap by continually shrinking the fiber air core.

   The fiber modes can also be classified by their polarization characteristics: the modes
are purely TE and TM for $m = 0$, but for $m \neq 0$ they are either TE-like or TM-like
(just like the EH and HE modes in conventional fibers). It turns out that the TM and
the TM-like modes with the lowest radial number are the last ones to remain in the
band gap as we shrink the core radius. For this reason only these modes and the TM
band structure (of the corresponding Bragg stack) are plotted in Fig. 2.

   In Fig. 2 we see that in the frequency window (0.705, 0.782) only the $m = 1$ mode
is present and form a band in the fundamental band gap. The segment of the band
with negative curvature or dispersion (i.e. $d^2\omega/d\beta^2 < 0$) is enclosed in the shaded
box spanning the frequency range (0.762, 0.782). Since both the angular frequency ω
and the propagation wave vector β have been normalized in Fig. 2, they need to be
"denormalized" before we can compare results with previous works. For instance, if we
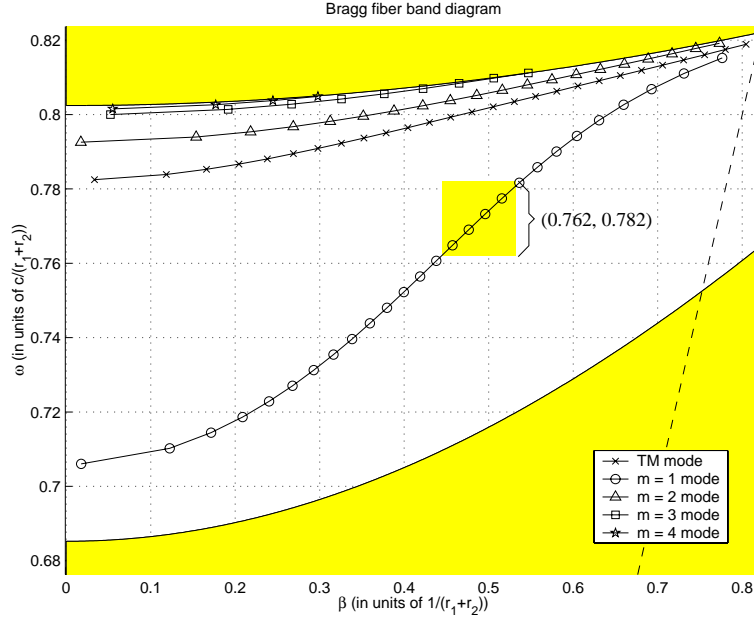
Fig. 2. Bragg fiber band diagram based on asymptotic computations. For clarity only the TM and TM-like modes with lowest radial number are plotted here, as all other modes have all been "pushed" out of the band gap. The TM band structure of the corresponding Bragg stack serves as the background and the dotted line shown is the light line. Boundary conditions are matched at the air core boundary. The structural parameters are given as follows: $n_1 = 4.6$, $n_2 = 1.5$, $r_1 = 10$, $r_2 = 2$, and $r_{core} = 30$, all in normalized units. Note in the frequency window (0.762, 0.782) the $m = 1$ band not only exhibits single-mode behavior but also possesses negative dispersion values.

pick the normalized operating frequency to be $0.77(c/(r_1 + r_2))$, which, when converted to 1.55μm in MKS units, gives a dispersion value D of roughly -25,000 ps/(nm.km), a 25-fold improvement over previous results. See Fig. 3 for a plot of the dispersion value D in the vicinity of the operating wavelength.

No optimization technique is used in plotting Fig. 2, which is simply the result of trial and error. The value of r_{core} is chosen to maximize the bandwidth of the single-mode window: too small of a core radius would push even the $m = 1$ mode outside the bandgap, whereas too big of a radius would introduce too many higher-order modes into the bandgap. r_1 and r_2 are also chosen based on similar considerations. As a general rule, we find that higher r_1/r_2 ratios lead to higher negative dispersion values. This however does not mean that we should let r_1/r_2 increase without bound, for the bandgap shrinks to zero as r_1/r_2 approaches infinity (Maximum bandgap occurs when the quarter wave condition is satisfied. Any deviation from it results in a reduced bandgap). This trade-off between single-mode bandwidth and dispersion value D gives our choice of r_1 and r_2 in Fig. 2.

3   Simulation results

We have already used the asymptotic algorithm to study the dispersion properties of a Bragg fiber in Sec. **2**. Now we use finite difference time domain (FDTD) simulations to verify the validity of our asymptotic approach. Note our inherently 3D structure can be reduced into a 2D one by extracting out the exponential z dependence. As a result, if we write the electric field as $\vec{E}(x, y, t)\exp(i\beta z)$ and the magnetic field as $\vec{H}(x, y, t)\exp(i\beta z)$,
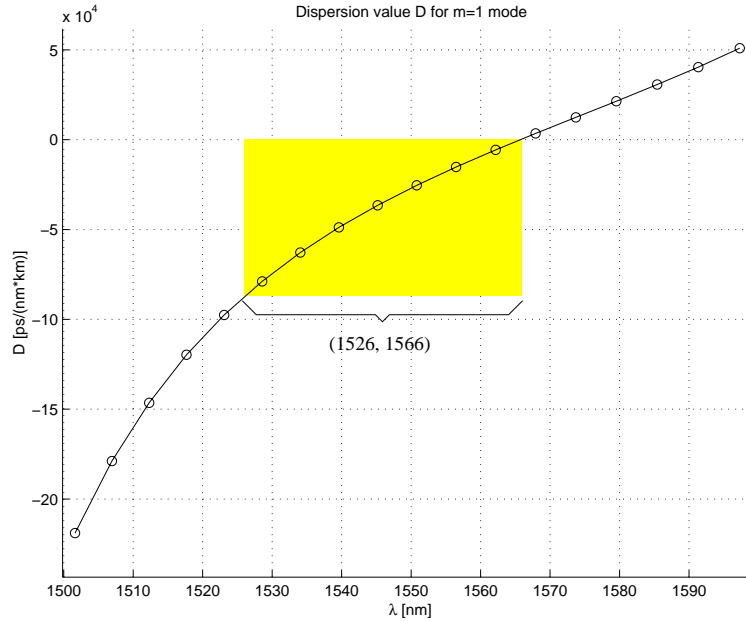
Fig. 3. Dispersion value D for the $m = 1$ band based on asymptotic computations. The second order derivative $\frac{\partial^2 \beta}{\partial \omega^2}$ is calculated by a direct differential method (i.e., no curve fitting is involved). Fiber structure and boundary matching surface follow those of Fig. 2. Shaded area (1526, 1566) is made to match the frequency window (0.762, 0.782) (also in Fig. 2) by choosing the normalized operating frequency to be $0.77(c/(r_1 + r_2))$, which translates to $1.55\mu m$ in MKS units. Note at $\lambda = 1.55\mu m$, dispersion value $D \approx -25,000ps/(nm.km)$.

the 3D Maxwell equations become:

$$(\nabla_\perp + i\beta\vec{e}_z) \times \vec{E}(x, y, t) = -\mu_0 \frac{\partial}{\partial t}\vec{H}(x, y, t) , \tag{1}$$

$$(\nabla_\perp + i\beta\vec{e}_z) \times \vec{H}(x, y, t) = \epsilon_0\epsilon(x, y)\frac{\partial}{\partial t}\vec{E}(x, y, t) , \tag{2}$$

where $\nabla_\perp$ is defined as $\vec{e}_x \frac{\partial}{\partial x} + \vec{e}_y \frac{\partial}{\partial y}$. We can transform these 2D differential equations into a set of finite difference equations following the standard finite difference time domain procedure [18]. At the boundaries of the computational domain, we use the perfectly matched layer boundary condition (PML) [19, 20] to absorb all the outgoing radiation. For the 2D FDTD equations and other details about the implementation of the algorithm, the reader should consult Ref. [21].

As in Sec. **2** we consider an air-core Bragg fiber with the following parameters: $r_{core} = 30$, $n_1 = 4.6$, $r_1 = 10$, $n_2 = 1.5$ and $r_2 = 2$, where the parameters are defined in Fig. 1. Twelve cladding pairs are used in our simulations to reduce the radiation loss to approximately 0.2dB/km [10].

To verify the dispersion curve in Fig. 2 with FDTD simulations, we first give the fiber an initial field and let it evolve in time in accordance with the Maxwell's equations, with the value of a chosen field component recorded at every time step. We then proceed to perform a fast Fourier transform (FFT) on the time evolution data, and each confined mode would be represented by a peak in the FFT plot in frequency spectrum.

Both the asymptotic and the FDTD results are shown in Fig. 4, where the asymptotic curve is simply copied over from Fig. 2. We find a good agreement between the two curves.
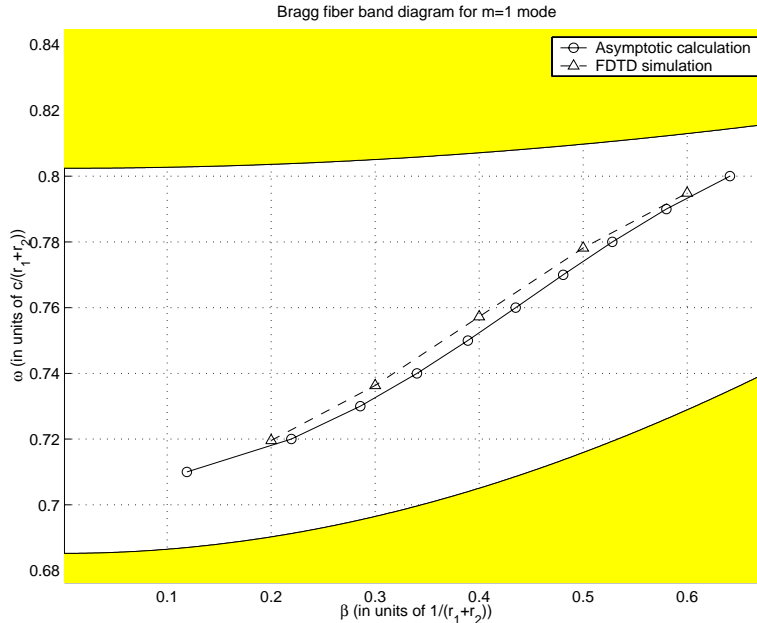
Fig. 4. Bragg fiber band diagram for the m=1 mode. The asymptotic curve is copied from Fig. 2 and the FDTD structure is defined with 12 cladding pairs.

In Fig. 5, we show the distribution of the H_z field obtained from FDTD calculations. The frequency and propagation constant of the mode are respectively $\omega = 0.777(c/(r_1 + r_2))$ and $\beta = 0.5(1/(r_1 + r_2))$. Fig. 5 clearly shows that the guided mode has a radial number $l = 0$ (no null in the radial direction inside the core), an azimuthal number $m = 1$ and a significant portion of the field concentrated within the air core.

4 Observations and comments

In Sec. **2** we found a frequency window in which only the $m = 1$ mode can propagate. This claim was made, however, based on asymptotic calculations that matched the boundary conditions at the air core boundary (i.e., only one layer in the IR). Would the claim still hold true as we include more layers in the IR, which, as Ref. [10] shows, would improve the accuracy of the solutions? The answer is an unfortunate 'No': given sufficient number of cladding layers we have found numerous higher-order cladding modes in the above-mentioned single mode frequency window. One such higher-order mode is plotted in Fig. 6, which is found by matching the boundary conditions at the outer surface of the 50th layer (i.e., the IR contains 50 layers). This $m = 4$ band cuts through the frequency window (0.762,0.782), rendering it multi-mode. The $m = 1$ curve is also redrawn under this new boundary matching condition and it does not change much from Fig. 2. In fact our calculations show that as we move the boundary-matching surface from the air core boundary to the 50th cladding layer, the $m = 1$ band converges very quickly from the band in Fig. 2 to the one in Fig. 6. Moving the boundary-matching surface further out into the cladding region would be unnecessary as it would result in only a minimal correction to Fig. 6. Thus we can regard the $m = 1$ band in Fig. 6 as the exact mode solutions and work out the "exact" dispersion value D at the same frequency of $0.77(c/(r_1 + r_2))$, which turns out to be roughly -20,000 ps/(nm.km).

Just as a side note, the $m = 4$ band in Fig. 6 is not the same as the one in Fig. 2. In fact, as we move the boundary-matching surface from the air core boundary to the
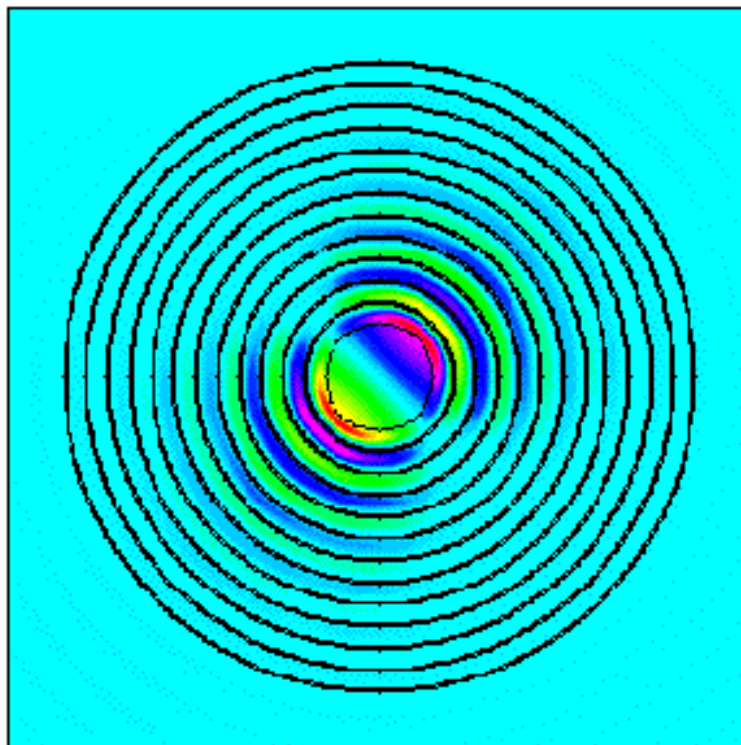
Fig. 5. The H_z field distribution of an $m = 1$ mode based on FDTD simulation. The parameters of the Bragg fiber are given in the caption of Fig. 2. The Bragg cladding consists of 12 cladding pairs and the whole fiber is immersed in air. The frequency and propagation constant of the mode are respectively $\omega = 0.777(c/(r_1 + r_2))$ and $\beta = 0.5(1/(r_1 + r_2))$.

50th cladding layer, the $m = 4$ mode in Fig. 2 gradually moves up in frequency and eventually disappears from the bandgap. In other words, its presence in Fig. 2 is merely a result of numerical errors inherent in our asymptotic calculations.

Single mode transmission would seem to be unrealizable if not for the following considerations:

(1) Just like the cladding modes in conventional fibers, the higher-order cladding modes in Bragg fibers also have a much more spread-out field profile than the $m = 1$ modes, which translates into higher loss for fibers with fixed number of cladding layers. This is also manifested in the fact that our first round of asymptotic calculations (by matching boundary conditions at the air core boundary) failed to detect any of the higher-order modes, due to large computation errors incurred by the asymptotic approximations. Theoretically this means we can classify the Bragg fiber modes into two categories based on their confinement characteristics: those of truly confined air-core modes and those of less confined cladding modes. In Ref. [10] we pointed out that Bragg fibers are not true Bragg structures due to their lack of translational periodicity. Rather, we can view them as Bragg structures with distributed perturbations, with the amount of perturbation decaying to zero as $r \to \infty$. Since the asymptotic calculations assume true Bragg confinement after the boundary-matching surface, then any modes that can be detected by matching the boundary conditions at the air core boundary is confined by true Bragg reflections, whereas all the other modes require at least some distributed perturbations to achieve confinement.
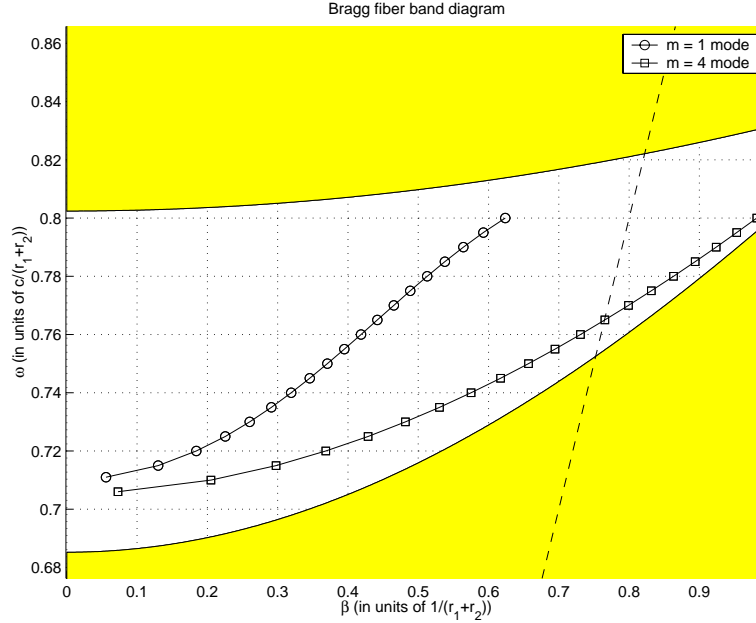
Fig. 6. Bragg fiber band diagram based on asymptotic computations. Just as in Fig. 2, only the TM-like bands with the lowest radial number are plotted. Boundary conditions are matched at the 50th cladding layer. The fiber structural parameters are given in the caption of Fig. 2. Note that the $m = 4$ band was missing in Fig. 2.

A more precise comparison is made in Fig. 7, in which the field profiles of both the $m = 1$ and $m = 4$ modes are plotted at the operating frequency. We find that the $m = 1$ mode is much more confined that the higher-order mode.

(2) Modes of different azimuthal symmetries are orthogonal. If the incoming fiber is properly aligned with the Bragg DCF, then the incident $m = 1$ mode would theoretically only excite the $m = 1$ mode in the Bragg fiber. Of course in practice fiber misalignment and material imperfections would never allow excitation of $m = 1$ mode alone in the DCF, but we believe it could still be a contributing factor that we can take advantage of.

In our FDTD simulations described in Sec. **3**, no higher-order cladding modes have ever been detected. This is probably due to both large radiation losses and selective mode excitation by the initial field, confirming the validity of the two arguments above (Given enough cladding layers and a proper initial field, higher-order modes like the $m = 4$ mode in Fig. 6 can be found using FDTD simulations and the results agree well with that given by the asymptotic approach).

We want to point out again that this paper represents only a theoretical study of the dispersion properties of Bragg fibers and does not represent a design of a realistic dispersion-compensating fiber. In this paper we only aim to show the possibility of achieving large negative dispersion through Bragg reflections. The choice of large index contrast in the cladding layers is a mere convenience. It not only affords us a large band gap to work with, but through tight mode confinement also allows us to verify our asymptotic calculations within a reasonable time frame using FDTD simulations. In fact our calculations show that the large negative dispersion value obtained is a direct consequence of Bragg reflection and its order of magnitude does not depend on the index contrast. Also note the material dispersion is deliberately left out of our calculations and simulations, as it depends on the particular choice of materials.
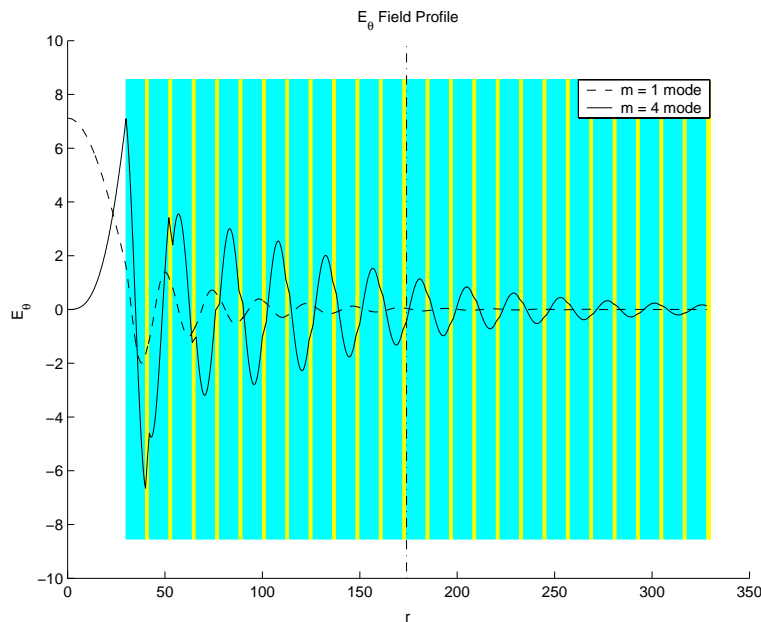
Fig. 7. The radial profile of E_θ field of guided Bragg fiber modes. The white area is the fiber core and the shaded layers represent the cladding layers. All structural parameters are given in the caption of Fig. 2. The vertical dashed line shows the boundary of a fiber structure with 12 cladding pairs, used in the FDTD simulations in Sec. **3**. The frequency of the mode is $\omega = 0.77(1/(r_1 + r_2))$, the chosen normalized operating frequency.

5 Future Work

Can we build a realistic dispersion-compensating fiber as it is? The answer is "No". Though Bragg fibers with large index contrast have in fact been made [2], with the high-index layer made of Tellurium (n = 4.6), such a high-index material suffers from an absorption loss that is generally several orders of magnitude higher than that of glass, hence makes them unusable in long-haul communication systems. Besides, the structural parameters of the Bragg fiber used in this paper are not compatible with the fiber parameters used in the real world. For example, if the normalized frequency of $0.77(c/(r_1 + r_2))$ is converted to the operating wavelength $\lambda = 1.55\mu m$, then the fiber core radius r_{core} works out to be roughly 0.47μm (with $r_1 = 0.16\mu m$, and $r_2 = 0.032\mu m$ respectively), which is one order of magnitude smaller than that of a conventional fiber core, hence a huge splicing loss would result. One possible way to get around these problems is to reduce the index contrast between the cladding layers. The problem, however, is that Bragg fibers of low index contrast require a large number of cladding layers for mode confinement. For example, Bragg fibers with an index contrast of 0.1 in the cladding layers require about 1,000 cladding pairs to achieve 0.2 dB/km loss [10], which poses a serious problem to fiber manufacturers. Research on reducing the number of cladding layers required for low-index fibers would be the subject of a future paper.

As a final remark, we note that in this paper we have only concerned ourselves with the dispersion value D, and ignored the other important figure of merit for dispersion compensation, namely, the dispersion slope. This is so because (1) we believe that in a realistic Bragg DCF with low index contrast, the single-mode bandwidth would be so small (due to a very narrow bandgap) that multi-channel compensation is unlikely. (2) there is actually a frequency at which the dispersion D "bottoms out", i.e., dispersion

slope is zero at this point. For the Bragg fiber in Fig. 2, this zero-slope point is located well above the the single-mode window, and hence is not shown in Fig. 3. Luckily, we have observed a sizable downward shift in its frequency as we reduce the index contrast, which should work in our favour when we develop the DCF with low index contrast. Once again, the details will be published in a future paper.

6   Conclusions

In this paper, we studied the dispersion property of the $m = 1$ mode in an air core Bragg fiber, which lends itself well to dispersion compensation owing to reduced absorption loss and nonlinear effects. Based on asymptotic calculations we showed large negative dispersion values can be achieved and the accuracy of the algorithm has been verified by FDTD simulations.

7   Acknowledgments